VI International Conference on Computational Methods for Coupled Problems in Science and Engineering
COUPLED PROBLEMS 2015
B. Schrefler, E. Oñate and M. Papadrakakis (Eds)

MODELLING OF ELECTROMAGNETIC BREAKING AND ELECTROMAGNETIC STIRRING IN THE PROCESS OF CONTINUOUS CASTING OF STEEL

KATARINA MRAMOR[*], ROBERT VERTNIK [†] AND BOŽIDAR ŠARLER [*†]

[*] Laboratory for Multiphase Processes (LMP)
University of Nova Gorica
Vipavska 13, 5000 Nova Gorica, Slovenia
e-mail: katarina.mramor@ung.si, www.ung.si

[†] Institute for Metals and Technology (IMT)
Lepi pot 11, 1000 Ljubljana, Slovenia
e-mail: bozidar.sarler@imt.si, www.imt.si

Key words: Continuous Casting, Electromagnetic Breaking, Electromagnetic Stirring, Meshless Methods.

Abstract. More than 95 % of crude steel is nowadays processed by Continuous Casting (CC) [1]. To further advance the quality of the products and efficiency of the process, electromagnetic (EM) field, which affects the fluid flow as well as the temperature and segregation is added to the CC process. In general, there are two types of electromagnetic devices applicable to the CC process; the electromagnetic breakers (EMBR) which employ the direct current, and the electromagnetic stirrers (EMS), which employ the alternating current. Which of the devices is employed depends on what are the desired effects. Both of the processes are modelled by implementing the Lorentz force into the momentum equation, and if necessary, the Joule heating term into the energy equation. However, the way how these two terms are modelled, depends on the type of the implemented device. In case of EMBRs, the assumption of low magnetic Reynolds number Re_m is made, and consequently, the current density is calculated by solving the Poisson's equation for the electric potential. The EMSs on the other hand, require a low-frequency approximation and the solution of induction equation. The complete set of governing equations for CC process [2] under the influence of magnetic field includes mass, momentum, energy, and species transfer equations, and Maxwell's equations together with Ohm's law and charge conservation equation. Additionally, the turbulent kinetic energy and dissipation rate equations together with Abe-Kondoh-Nagano closures are used to account for the turbulence, the lever rule model is used to model the microsegregation, the mixture continuum model is used to model the macrosegregation, fractional step method is used to model pressure-velocity coupling and the enthalpy-temperature relation is used to calculate the temperature from the enthalpy. The solution is sought for on a five-nodded local subdomains by constructing an approximation with multiquadric radial basis functions as a basis and collocation to find the expansion coefficients [3,4]. Present paper presents the discretization of governing equations, together with boundary conditions for both EMBR and EMS devices with meshless Local Radial Basis Function Collocation Method (LRBFCM) [5].

1 INTRODUCTION

The modelling of application of magnetic field to the continuous casting process started as early as 1982 [6]. In 1986 [7], the 3D flow field with a rotational EMS of round steel strand was calculated, allowing to examine the influence of the stirrers position, the stirring length and EM parameters on the flow field. The first computational 3D study of EMBR systems was performed in 1982 [8]. The modelling of solidification and solute distribution was added to the model in 1998 [9]. The model considers the blockage of fluid flow by columnar dendrites in the mushy zone, the change in liquidus temperature with liquid concentration and the double diffusive convection. Turbulence of molten steel flow was modelled by $k-\varepsilon$ turbulence model in [7, 10], followed by steady Reynolds-Averaged Navier-Stokes (RANS) models [11], filtered unsteady RANS model [11], Large Eddy Simulation (LES) models [11, 12, 13] and RANS Shear Stress (RANS-SST) model [14].

The most common numerical methods used in computational modelling of continuous casting of steel are Finite Difference Method (FDM) [15, 16], Finite Volume Method (FVM) [17, 18] and Finite Element Method (FEM) [19, 20]. As the geometry in the continuous casting process is complex and the physical system requires moving and/or deforming boundaries, the mesh generation can present a substantial problem for the above mentioned numerical methods. To circumvent this problem, also meshless numerical methods have recently been considered for this problem. Among various available meshless methods, such as meshless local Petrov-Galerkin method [21], point interpolation method [22], method of fundamental solutions [23], etc., LRBFCM [5] has been chosen to tackle the problem under consideration. This method has first been applied to the CC problem in 2011 [24]. Lately, the application of magnetic field [3, 4] has been added to the model. The next step will be the application of macrosegregation [25] to the already existing heat transfer and fluid flow model of CC.

The strength of magnetic field is calculated analytically and depends on the strand distance, the number of windings in the coils, the size of the windings, and the electric current. In the present paper the discretization of governing equations or EMBR and EMS devices is presented.

2 GOVERNING EQUATIONS

The continuous casting process with applied magnetic field can be described by five conservation equations; namely the mass, momentum, energy, species and charge conservation equations,

$$\nabla \cdot \mathbf{v} = 0 \tag{1}$$

$$\frac{\partial(\rho \mathbf{v})}{\partial t} + \nabla \cdot (\rho \mathbf{v}\mathbf{v}) = -\nabla p + \nabla \cdot \left[\left(\mu_L + \mu_t \frac{\rho}{\rho_L} \right) \left[\nabla \mathbf{v} + (\nabla \mathbf{v})^T \right] \right] - \frac{2}{3} \nabla(\rho k) - \tag{2}$$

$$- \mu_L \frac{K_0 (1 - f_L)^2}{f_L^3} (\mathbf{v} - \mathbf{v}_S) + \rho \mathbf{g} \left(\beta_T (T - T_{ref}) + \beta_C (C - C_{ref}) \right) + \mathbf{j} \times \mathbf{B}$$

$$\frac{\partial(\rho h)}{\partial t}+\nabla\cdot\left(\rho\mathbf{v}h\right)=\nabla\cdot\left(\lambda\nabla T\right)+\nabla\cdot\left(\rho f_S\left(h_L-h_S\right)(\mathbf{v}-\mathbf{v}_S)\right)+ \\ +\nabla\cdot\left(f_L\frac{\rho_L\nu_t}{\sigma_t}\nabla h_L\right)+\frac{|\mathbf{j}|^2}{\sigma_0} \tag{3}$$

$$\frac{\partial(\rho C)}{\partial t}+\nabla\cdot\left(\rho C\mathbf{v}\right)=\nabla\cdot\left(\rho f_S D_S\nabla C_S+\rho f_L D_L\nabla C_L\right)+ \\ +\nabla\cdot\left(\rho(C_L-C)(\mathbf{v}-\mathbf{v}_S)\right)+\nabla\cdot\left(\frac{f_L\mu_t}{\sigma_C}\nabla C_L\right) \tag{4}$$

$$\nabla\cdot\mathbf{j}=-\frac{\partial\rho_e}{\partial t}=0 \tag{5}$$

where $\mathbf{v}$ stands for the velocity of the mixture, $\rho=\rho_S=\rho_L$ is the density, assumed to be constant and equal in both phases. t stands for time and p for pressure. μ_t is turbulent viscosity and μ_L is the dynamic viscosity, k represents turbulent kinetic energy and K_0 is the permeability constant. $\mathbf{v}_S$, β_T, β_C, $\mathbf{g}$, T, T_{ref}, C, and C_{ref} represent velocity of solid phase, thermal expansion coefficient, solute expansion coefficient, gravitational acceleration, temperature, reference temperature, species concentration and reference species concentration, respectively. $\mathbf{j}\times\mathbf{B}$ is Lorentz force, and is in detail described below. h stands for enthalpy, λ for thermal conductivity, and σ_0 for electrical conductivity. f_S, f_L, h_S, and h_L represent solid volume fraction, liquid volume fraction, enthalpy of the solid phase and enthalpy of the liquid phase, and ν_t is turbulent kinematic viscosity. D_S, and D_L are diffusion coefficients for solid and liquid phase respectively. ρ_e and $\mathbf{j}$ are electric charge density and current density. C_S and C_L are the concentration of solute in solid and liquid phase, respectively. Level rule microsegregation model is used to determine the liquid fraction, structured with

$$f_L=1-\frac{1}{1-k_p}\frac{T-T_L}{T-T_m}, \tag{6}$$

the partition ratio

$$k_p=\frac{C_S}{C_L}, \tag{7}$$

the liquidus temperature

$$T_L=T_m+(T_e-T_m)\frac{C}{C_e}, \tag{8}$$

and the concentration of solute in liquid phase

$$C_L=\frac{C}{1+f_S(k_p-1)}. \tag{9}$$

T_m, T_e, and C_e are the melting temperature, the eutectic temperature and the eutectic solute concentration, respectively.

Additionally, the turbulent kinetic energy and the dissipation rate equations are added to account for the turbulence

$$\frac{\partial(\rho k)}{\partial t}+\nabla\cdot\left(\rho\mathbf{v}k\right)=\nabla\cdot\left[\left(\mu_L\frac{\rho}{\rho_L}+\frac{\mu_t}{\sigma_k}\right)\nabla k\right]+P_k+G_k-\rho\varepsilon \\ -\rho D_{k-\varepsilon}+\mu_L\frac{K_0\left(1-f_L\right)^2}{f_L^3}\frac{\rho}{\rho_L}k \tag{10}$$

$$\frac{\partial(\rho\varepsilon)}{\partial t}+\nabla\cdot\left(\rho\mathbf{v}\varepsilon\right)=\nabla\cdot\left[\left(\mu_L\frac{\rho}{\rho_L}+\frac{\mu_t}{\sigma_\varepsilon}\right)\nabla\varepsilon\right]+\rho E_{k-\varepsilon}- \\ -\mu_L\frac{K_0\left(1-f_L\right)^2}{f_L^3}\varepsilon+\left[c_{1\varepsilon}f_1\left(P_k+c_{3\varepsilon}G_k\right)-c_{2\varepsilon}f_2\rho\right]\frac{\varepsilon}{k} \tag{11}$$

where ε stands for the dissipation rate, σ_t, σ_C, σ_k, σ_ε, $c_{1\varepsilon}$, f_1, $c_{2\varepsilon}$ and f_2 are closure coefficients. P_k, G_k, $D_{k-\varepsilon}$, and $E_{k-\varepsilon}$ are the shear production of turbulent kinetic energy, generation of turbulence due to the buoyancy force, source term in k equation and source term in ε equation, respectively. Abe-Kondoh-Nagano closures are used [26].

Maxwell's equations together with Ohm's law are used to calculate the magnetic field effects

$$\nabla\cdot\mathbf{E}=\frac{\rho_e}{\varepsilon_0}, \tag{12}$$

$$\nabla\cdot\mathbf{B}=0, \tag{13}$$

$$\nabla\times\mathbf{E}=-\frac{\partial\mathbf{B}}{\partial t}, \tag{14}$$

$$\nabla\times\mathbf{B}=\mu_0\left(\mathbf{j}+\varepsilon_0\frac{\partial\mathbf{E}}{\partial t}\right), \tag{15}$$

$$\mathbf{j}=\sigma(-\nabla\phi+\mathbf{v}\times\mathbf{B}), \tag{16}$$

where $\mathbf{E}$, ε_0, $\mathbf{B}$, and μ_0 are electric field, permittivity of free space, magnetic field density, and permeability of free space. The extent of coupling between the magnetic field and velocity, temperature, species concentration or energy, depends on the device (EMBR or EMS) that is used to produce the EM field. The coupling in both cases is done through the Lorentz force

$$\mathbf{F}_m=\mathbf{j}\times\mathbf{B}, \tag{17}$$

which is added to the momentum equation and Joule heating term

$$\frac{|\mathbf{j}|^2}{\sigma_0}, \tag{18}$$

that is added to the energy equation.

3 ELECTROMAGNETIC FIELD EQUATIONS

Both the EMBR and EMS are incorporated into the model through the Lorentz force, and if necessary, the Joule heating term. However, the magnetic field and consequently the Lorentz force for each of the EM devices are calculated in a different way. The calculation procedure is outlined below. In both, EMS and EMBR cases, an assumption of low $\mathrm{Re}_m=vL\mu_0\sigma_0$ is made. v

is the characteristic velocity and L is the characteristic length. The solution of EMS additionally requires a low frequency approximation.

3.1 Electromagnetic braking

The considered device for EMBR consist of two coils facing in the same direction as schematically presented in Figure 1. This coil configuration consists with EMBR ruler. The magnetic field for such coil arrangement can be calculated analytically [27, 28] by first calculating the magnetic field components of each individual winding

$$B_x = \frac{\mu_0 I}{4\pi}\sum_{i=1}^{4}\left[\frac{(-1)^i z_i}{r_i(r_i+(-1)^{i+1}y_i)} - \frac{y_i}{r_i(r_i+z_i)}\right] \tag{19}$$

$$B_y = \frac{\mu_0 I}{4\pi}\sum_{i=1}^{4}\frac{(-1)^{i+1}x}{r_i(r_i+z_i)} \tag{20}$$

$$B_z = \frac{\mu_0 I}{4\pi}\sum_{i=1}^{4}\frac{(-1)^{i+1}x}{r_i(r_i+(-1)^{i+1}y_i)} \tag{21}$$

where x, $y_{1,3} = y + \frac{a}{2}$, $y_{2,4} = y - \frac{a}{2}$, $z_{1,2} = z + \frac{b}{2}$, $z_{3,4} = z - \frac{b}{2}$, $r_i = \sqrt{x^2 + y_i^2 + z_i^2}$. The assumption of tightly wound loops placed next to each other is then made. By substituting $x \to x + n \cdot \phi_w$, $y \to y + m \cdot \phi_w$ and $z \to z + m \cdot \phi_w$, where n, m, and ϕ_w are the number of loops in x direction, the number of loops in y and z directions and the diameter of the wire, the total field of a single solenoid coil is obtained by summing up all of the contributions

$$\mathbf{B} = \mathbf{B}_1 + \ldots + \mathbf{B}_N . \tag{22}$$

The parallel coil configuration is obtained by employing a transformation $x \to x + \frac{d}{2}$ and $x \to x - \frac{d}{2}$, where d is the distance between coils, and the summation of both contributions is $\mathbf{B} = \mathbf{B}_{-\frac{d}{2}} + \mathbf{B}_{+\frac{d}{2}}$.

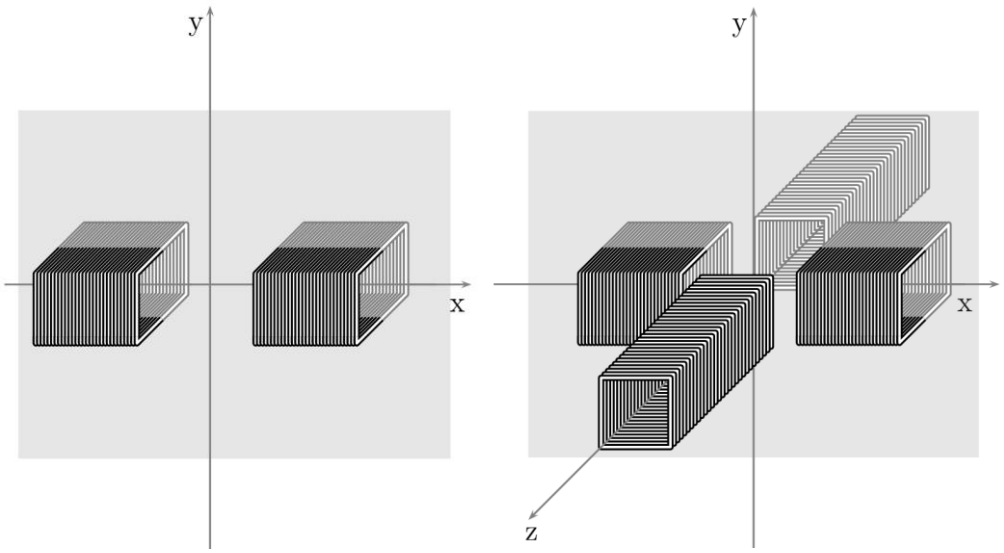

Figure 1: Left: Scheme of EMBR configuration. Right: Scheme of EMS configuration.

The magnetic field is then inserted into the electric potential equation

$$\nabla^2\phi = \nabla\cdot(\mathbf{v}\times\mathbf{B}) \tag{23}$$

which is obtained by inserting Ohm's law (Eq. 9) into the charge conservation equation (Eq. 5). Once the electric potential is calculated, it is inserted into Eq. 9 in order to obtain the current density, which is then used to calculate Lorentz force and, if needed, Joule source term.

3.2 Electromagnetic stirring

The considered device for EMS consists of four coils facing each other. The coils employ alternating current to produce a time varying magnetic field. By introducing the vector $\mathbf{A}$ and scalar ϕ potentials and enforcing the Coulomb gauge condition ($\nabla\cdot\mathbf{A}=0$), the magnetic and the electric fields are rewritten as

$$\mathbf{B} = \nabla\times\mathbf{A}\,, \tag{24}$$

$$\mathbf{E} = -\nabla\phi - \frac{\partial\mathbf{A}}{\partial t}\,. \tag{25}$$

Inserting Eqs. (24) and (25) into Maxwell's equations (Eqs. 12-15), the following equations are obtained

$$\nabla^2\mathbf{A} = \mu_0\sigma_0\frac{\partial\mathbf{A}}{\partial t} - \mu_o\sigma_0\mathbf{v}\times(\nabla\times\mathbf{A}) - \mu_0\sigma_0\nabla\phi\,, \tag{26}$$

$$\nabla^2\phi = 0\,, \tag{27}$$

and consequently, ϕ can be set to $\phi = const.$ By applying the Ohm's law, Eq. 26 can be expressed as

$$\nabla^2 \mathbf{A} = -\mu_0 (\mathbf{j}_{ind} + \mathbf{j}_{ext}), \tag{28}$$

where $\mathbf{j}_{ind}$ and $\mathbf{j}_{ext}$ are induced and imposed currents, respectively. The solution of thus obtained linear system of equations can be further simplified by taking into account that the imposed current density is harmonic and can therefore be written as

$$\mathbf{j}_{ext} = \mathbf{j}_{ext}(\mathbf{r}) e^{i\omega t}, \tag{29}$$

where $\mathbf{j}_{ext}(\mathbf{r})$ is the amplitude of current density in the coils and ω is the source frequency [29, 30]. The Lorentz force and, if necessary, the Joule source terms are calculated as a real part of the complex fields.

4 DISCRETIZATION OF GOVERNING EQUATIONS

The discretization procedure of LRBFCM is discussed in the continuation of the present paper. As all the governing equations follow the conservation principle, they can be described with a general transport equation as

$$\frac{\partial(\rho\Phi)}{\partial t} + \nabla \cdot (\rho \mathbf{v} \Phi) = \nabla \cdot (D \nabla \Phi) + S_\Phi, \tag{30}$$

where D is diffusion coefficient, Φ is general dependent variable (e.g. velocity) and S_Φ a source term. The first term on the left side in the equation is called the transient term, whereas the second term is the convection term. On the right side, the first term is the diffusion term. The description of discretization is demonstrated for a general transport equation, as the discretization of mass, momentum, energy, species conservation, turbulent kinetic energy and dissipation rate governing equations follows the same principle.

4.1 Time discretization

The time discretization is performed by explicit first-order approximation (explicit Euler) scheme. The transient term (first term in Eq. 30) is thus rewritten as

$$\frac{\partial(\rho\Phi)}{\partial t} \approx \frac{\rho(t_0 + \Delta t)\Phi(t_0 + \Delta t) - \rho(t_0)\Phi(t_0)}{\Delta t} = \frac{\rho\Phi - \rho_0\Phi_0}{\Delta t} \approx \rho_0 \frac{\Phi - \Phi_0}{\Delta t} \tag{31}$$

where $\Phi(t_0 + \Delta t)$ and $\Phi(t_0)$ represent the value of sought for variable at time $t_0 + \Delta t$ and t_0, respectively, and ρ_0 represents the value of density at time t_0.

4.2 Space discretization

Space discretization in LRBFCM is done by collocation with RBFs. The general idea behind this method is to construct an approximation function on the local group of nodes, the so-called influence domains, and to apply the PDE on the approximation functions in a strong formulation. The approximation function Φ is constructed on a local subdomain $_l$ and is represented as a linear combination of weighted basis functions $_l\psi_i$

$$ {}_l\Phi(\mathbf{p}) = \sum_{i=1}^{N_{basis}} {}_l\psi_i(\mathbf{p}) {}_l\alpha_i , \tag{32} $$

where ${}_l\alpha_i$, N_{Basis}, ${}_l\psi_i$, and $\mathbf{p} = x\mathbf{i}_x + y\mathbf{i}_y + z\mathbf{i}_z$ are the expansion coefficient, the number of basis functions, the basis function, and the position vector in influence domain ${}_l$, where $l = 1,\ldots,N_{domain}$, respectively. The position vector is expressed in Cartesian coordinate system with coordinates x, y, z and base vectors $\mathbf{i}_x, \mathbf{i}_y, \mathbf{i}_z$. Among the various possible basis functions, such as polynomials, Fourier basis functions, the multiquadric RBFs are chosen

$$ \psi(r) = \sqrt{r^2 + c^2} , \tag{33} $$

where ${}_l r_j = \| \mathbf{p} - {}_l\mathbf{p}_j \| = \sqrt{\left(\frac{x - {}_l x_j}{{}_l x_{max}}\right)^2 + \left(\frac{y - {}_l y_j}{{}_l y_{max}}\right)^2 + \left(\frac{z - {}_l z_j}{{}_l z_{max}}\right)^2}$ is the distance between the central node $\mathbf{p}$ and the support node ${}_l\mathbf{p}_j$ and c is the shape parameter. The distances between the current position $\mathbf{p}$ and the support nodes in the influence domain region are normalized by the maximum lengths in subdomain ${}_l x_{max}$, ${}_l y_{max}$, and ${}_l z_{max}$. This allows to use a constant value of ($c = 32$) in differently arranged subdomains. The expansion coefficients of the approximation function are determined by collocation, which demands that the number of basis functions equals the number of the domain nodes. The collocation condition $\Phi({}_l\mathbf{p}_j) = {}_l\Phi_j$ must hold for all the points in the influence domain. By implementing the collocation condition, a linear system of equations is obtained

$$ {}_l\boldsymbol{\psi}\, {}_l\boldsymbol{\alpha} = {}_l\underline{\Phi} , \tag{34} $$

where ${}_l\boldsymbol{\psi}$, ${}_l\boldsymbol{\alpha}$, and ${}_l\underline{\Phi}$ are the matrix of RBFs, the vector of the expansion coefficients, and the vector of corresponding data values, respectively. If the matrix is non-singular [31], the expansion coefficients can be obtained as

$$ {}_l\boldsymbol{\alpha} = {}_l\boldsymbol{\psi}^{-1}\, {}_l\underline{\Phi} . \tag{35} $$

The approximation function thus becomes

$$ {}_l\Phi(\mathbf{p}) = \sum_{i=1}^{N_{Basis}} {}_l\psi_i(\mathbf{p}) \sum_{j=1}^{N_{Basis}} {}_l\psi_{ij}^{-1}(\mathbf{p})\, {}_l\Phi_j . \tag{36} $$

The convection term is first rewritten as

$$ \nabla\cdot(\rho\mathbf{v}\Phi) = \Phi\nabla\cdot(\rho\mathbf{v}) + \rho\mathbf{v}\nabla\cdot\Phi \tag{37} $$

and spatial discretization is then applied to each of the terms separately. The first term is rewritten as

$$ \left[\Phi\nabla\cdot(\rho\mathbf{v})\right]_l \approx \Phi \sum_{i=1}^{N_{Basis}} \frac{\partial}{\partial x_j} {}_l\psi_i \sum_{n=1}^{N_{Basis}} {}_l\psi_{in}^{-1}\, {}_l(\rho\mathbf{v})_n \tag{38} $$

and the second term as

$$(\rho \mathbf{v} \nabla \cdot \Phi)_l \approx \rho \mathbf{v} (\sum_{i=1}^{N_{domain}} \frac{\partial}{\partial x_j} {}_l\psi_i \sum_{n=1}^{N_{domain}} {}_l\psi_{in}^{-1} {}_l\Phi_n) . \tag{39}$$

In the present case, only the second term (Eq. 39) is calculated, as the density is considered constant. Similarly, the diffusion term is first rewritten as

$$\nabla \cdot (D \nabla \Phi) = \nabla D \cdot \nabla \Phi + D \nabla^2 \Phi , \tag{40}$$

where D is a diffusion coefficient. The first term in Eq. (40) is discretized as

$$(\nabla D \cdot \nabla \Phi)_l \approx (\sum_{i=1}^{N_{domain}} \frac{\partial}{\partial x_j} {}_l\psi_i \sum_{n=1}^{N_{domain}} {}_l\psi_{in}^{-1} {}_lD_n) \cdot (\sum_{i=1}^{N_{domain}} \frac{\partial}{\partial x_j} {}_l\psi_i \sum_{n=1}^{N_{domain}} {}_l\psi_{in}^{-1} {}_l\Phi_n) \tag{41}$$

and the second as

$$(D \nabla^2 \Phi)_l \approx D_l \sum_{i=1}^{N_{Basis}} \frac{\partial^2}{\partial x_j^2} {}_l\psi_i \sum_{n=1}^{N_{Basis}} {}_l\psi_{in}^{-1} {}_l\Phi_n . \tag{42}$$

By using the above described procedure for time and space discretization, a general transport equation (Eq. 31) becomes

$$\begin{aligned} \Phi(t_0 + \Delta t)_l = \Phi(t_0)_l + \frac{\Delta t}{\rho_0} \Big(& \Phi \sum_{i=1}^{N_{Basis}} \frac{\partial}{\partial x_j} {}_l\psi_i \sum_{n=1}^{N_{Basis}} {}_l\psi_{in}^{-1} {}_l(\rho_0 \mathbf{v})_n - \\ & - \rho_0 \mathbf{v} (\sum_{i=1}^{N_{Basis}} \frac{\partial}{\partial x_j} {}_l\psi_i \sum_{n=1}^{N_{Basis}} {}_l\psi_{in}^{-1} {}_l\Phi_n) + \\ & + (\sum_{i=1}^{N_{Basis}} \frac{\partial}{\partial x_j} {}_l\psi_i \sum_{n=1}^{N_{Basis}} {}_l\psi_{in}^{-1} {}_lD_n) \cdot (\sum_{i=1}^{N_{Basis}} \frac{\partial}{\partial x_j} {}_l\psi_i \sum_{n=1}^{N_{Basis}} {}_l\psi_{in}^{-1} {}_l\Phi_n) + \\ & + D_l \sum_{i=1}^{N_{Basis}} \frac{\partial^2}{\partial x_j^2} {}_l\psi_i \sum_{n=1}^{N_{Basis}} {}_l\psi_{in}^{-1} {}_l\Phi_n + {}_l S_\Phi \Big)_0 \end{aligned} . \tag{43}$$

4.3 Discretization of Poisson equations

The discretization of Poisson's equation is a boundary value problem, whereas the previously described discretization is an initial value problem. Respectively, its discretization by LRBFCM is described separately. It is used for the solution of electric scalar potential in EMBR (Eq. 23), vector potential in EMS (Eq. 28), and pressure in FSM method, which is used for coupling of the mass conservation with the momentum conservation equations. A detailed description of FSM pressure-velocity coupling solution procedure and its implementation in the LRBFCM can be found in [2-5]. The discretization procedure for Poisson's equation is presented for a general variable. The global $\mathbf{p}_n$ and the local influence domain ${}_l\mathbf{p}_i$ nodes coincide and are connected by the following relation $\mathbf{p}_{n(l,i)} = {}_l\mathbf{p}_i$. The general variable is represented on each of the influence domains as a linear combination of basis functions and expansion coefficients as

$${}_l\Phi(\mathbf{p}) = \sum_{i=1}^{N_{domain}} \psi_{n(l,i)}(\mathbf{p}) \, {}_l\alpha . \tag{44}$$

The expansion coefficients are determined from collocation, as presented in Eq. 35. Φ is therefore determined in each of the subdomains as

$$ {}_l\Phi(\mathbf{p}) = \sum_{i=1}^{N_{Basis}} \sum_{j=1}^{N_{Basis}} {}_l\psi_{n(l,i)}(\mathbf{p})\, {}_l\Psi_{ij}^{-1} \Phi_{n,(l,j)} . \tag{45} $$

The discretized general Poisson equation is a result of collocation and application of Laplace operator in global node $\mathbf{p}_k$

$$ \sum_{k=1}^{N_{domain}} \Psi_{kl} \Phi_l = S_k , \tag{46} $$

where Ψ_{kl} is the sparse matrix element and S_k is a function of Φ. For scalar potential $S_k = \nabla \cdot (\mathbf{v} \times \mathbf{B})$, for vector potential $S_k = -\mu_0 (\mathbf{j}_{ind} + \mathbf{j}_{ext})$ and for pressure $S_k = \frac{\rho}{\Delta t} \nabla \cdot \mathbf{v}^*$, where $\mathbf{v}^*$ is the intermediate velocity.

4.4 Discretization of boundary conditions

In general, there are three types of boundary conditions: the Neumann, Dirichlet and Robin ones, all of which are used in the solution of governing equations for the CC of steel under the influence of magnetic field. The implementation of Dirichlet boundary conditions is straightforward

$$ {}_l\Phi(\mathbf{p}) = {}_l\,\Phi_{BC} . \tag{47} $$

The implementation of Neumann boundary conditions on the other hand requires the application of collocation

$$ \frac{\partial}{\partial \mathbf{n}} {}_l\Phi(\mathbf{p}) = \sum_{j=1}^{N_{domain}} \frac{\partial}{\partial \mathbf{n}} {}_l\psi_j(\mathbf{p})\, {}_l\alpha_j . \tag{48} $$

The same is true for Robin boundary conditions

$$ a \frac{\partial}{\partial \mathbf{n}} {}_l\Phi(\mathbf{p}) + b\, {}_l\Phi(\mathbf{p}) = \sum_{j=1}^{N_{domain}} \left(a \frac{\partial}{\partial \mathbf{n}} {}_l\psi_j(\mathbf{p}) + b\, {}_l\psi_j(\mathbf{p})\right) {}_l\alpha_j , \tag{49} $$

where $\mathbf{n}$ is normal to the boundary, and a and b are the weights.

5 CONCLUSIONS

In this paper, a local meshless procedure for discretization of governing equations and their boundary conditions for a coupled multiphysics problem, resulting from EMBR and EMS in CC is presented. The general local form of discretized equations is applied to the transport equations of mass, momentum, species, energy, turbulent kinetic energy and dissipation rate. The solution of Poisson's equation, which is representative for solving the electric vector potential and pressure Poisson's equation, is discretized. The discretisation results in solving of a global sparse matrix for all the nodes in calculation domain. In both cases the collocation with RBFs is used for local space discretization on influence domains and explicit Euler scheme is

used for time discretization. Several numerical results, stemming from the presented meshless computational scheme will be presented at the conference.

6 ACKNOWLEDGEMENTS

The research in this paper is sponsored by Slovenian Grant Agency under program group P2-0369 Modelling and Simulation of Materials and Processes and by the project L2-6775: Simulation of Industrial Solidification Processes under Influence of Electromagnetic Fields, co-sponsored by Štore Steel and IMPOL companies. The EMBR part of the research was sponsored by Centre of Excellence for Biosensors, Instrumentation and Process Control.

REFERENCES

[1] World Steel Association, *http: //www.worldsteel.org*, (2013).
[2] Vertnik, R. and Šarler, B. Solution of a continuous casting of steel benchmark test by meshless, *Eng. Anal. Bound. Elem.* (2014) **45**:45–1282.
[3] Mramor, K., Vertnik, R. and Šarler, B. Simulation of natural convection influenced by magnetic field with explicit local radial basis function collocation method, *Comp. Model. Eng. Sci.* (2013) **92**: 327–352.
[4] Mramor, K., Vertnik, R. and Šarler, B. Simulation of laminar backward facing step flow under magnetic field with explicit local radial basis function collocation method, *Eng. Anal. Bound. Elem.* (2006) **51:** 1269–1282.
[5] Šarler, B. and Vertnik, R. Meshfree explicit local radial basis function collocation method for diffusion problems, *Comp. Math. Appl.* (2006) **51**: 1269–1282.
[6] Birat, J.P. and Chone, J. Electromagnetic stirring on billet, bloom, and slab continuous casters: state of the art in 1982, *Iron. Steel.* (1982) **10**: 269–281.
[7] Spitzer, K. H., Dubke, M. and Schwerdtfeger, K. Rotational electromagnetic stirring in continuous casting of round strands, *Metal. Trans. B* (1986) **17**: 119–131.
[8] Yao, M., Ichimiya, M., Kiyohara, S., Suzuki. K.I., Mesaki, R., and Sugiyama, K. Three-dimensional analysis of molten metal flow in continuous casting mould. *Iron. Steel. Soc. Inc.* (1992) 123–129.
[9] Yang, H., Zhang, X., Deng, K., Li, W., Gan, Y., and Zhao, L. Mathematical simulation on coupled flow, heat, and solute transport in slab continuous casting process, *Metal. Mater. Trans. B* (1998) **29**: 1345–1356.
[10] Cukierski, K. and Thomas, B. G. Flow control with local electromagnetic braking in continuous casting of steel slabs, *Metal. Mater. Trans. B* (2008) **39**: 94-107.
[11] Chaudhary, R., Ji, C., Thomas, B.G., and Vanka, S. P. Transient turbulent flow in a liquid-metal model of continuous casting, including comparison of six different methods, *Metal. Mater. Trans. B* (2011) **42**: 987–1007.
[12] Chaudhary, R., Thomas, B.G., and Vanka, S. P. Effect of electromagnetic ruler braking (EMBr) on transient turbulent flow in continuous slab casting using large eddy simulations, *Metal. Mater. Trans. B* (2012) **43**: 532–553.
[13] Ji, C.-B., Li, J.-S., Yang, S.-F., and Sun, L.-Y. Large eddy simulation of turbulent fluid flow in liquid metal of continuous casting, *J. Iron. Steel. Res. Int.* (2013) **20**: 34–46.

[14] Miao, X., Timmel, K., Lucas, D., Ren, Z., Eckert, S., and Gerbeth, G. Effect of an electromagnetic brake on turbulent melt flow in a continuous casting mold, *Metal. Mater. Trans. B* (2012) **43**: 954–972.
[15] Özişik, M. N. *Finite Difference Methods in Heat Transfer.* CRC Press (1994).
[16] Wang, L., Shen, H., and Liu, B. Effect of electromagnetic field on fluid flow in continuous casting mold. *MCSP6-2004* (2004) 13-20.
[17] Zienkiewicz, O. C. and Taylor, R. L. *The Finite Element method*. McGraw Hill, Vol. I., (1989), Vol. II. (1991).
[18] Trinidade, L. B., Vilela, A. C. F., Vilhena, M. T. M. B., Soares, R. B. et al. Numerical model of electromagnetic stirring for continuous casting billets, *IEEE Trans. Mag.* (2002) **38**:3658-3660.
[19] Versteeg, H. K. and Malalasekera W. *An Introduction to Computational Fluid Dynamics: the Finite Volume Method*. Prentice Hall, (2007).
[20] Haiqi, Y., Baofeng, W., Huiqin, L., and Jianchao, L. Influence of electromagnetic brake on flow field of liquid steel in the slab continuous casting mold, *J. Mater. Process. Tech.* (2008) **202**:179-187.
[21] Atluri, S.N. and Zhu, T. A new meshless local Petrov-Galerkin (MLPG) approach in computational mechanics, *Comp. Mech.* (1998) **22**:117-127.
[22] Liu, G. R. and Gu, Y. T. A point interpolation method for two-dimensional solids, *Int. J. Numer. Method. Eng.* (2001) **50**:937-951.
[23] Golberg, M. A. and Chen, C. S. *Boundary Integral Methods-Numerical and Mathematical Aspects*. WIT Press, (1998).
[24] Vertnik, R. and Šarler, B. Local collocation approach for solving turbulent combined forced natural convection problems, *Adv. Appl. Math. Mech.* (2011) **3**:259-279.
[25] Kosec, G. and Šarler, B. Simulation of macrosegregation with mesosegregation in binary metallic casts by meshless method, *Eng. Anal. Bound. Elem.* (2014) **23**:189-204.
[26] Abe, K., Kondoh, T., and Nagano, Y. A new turbulence model for predicting fluid flow and heat transfer in separating and reattaching flows- I. Flow field calculations, *Int. J. Heat. Mass. Transf.* (1994) **37**:139-151.
[27] Li, T. T.-K. Tri-axial square Helmholtz coil for neutron EDM experiment, *Chinese Uni. Of Hong-Kong* - Report (2004) **1**: 1-23.
[28] Misakian, M. Equations for the magnetic field produced by one or more rectangular loops of wire in the same plane. *J. Res. Nat. Inst. Stand. Tech.* (2000) **105:**557-564.
[29] Maldovan, M., Príncipe, J., Sánchez, G., Pignotti, A. and Goldschmit, M. Numerical modeling of continuous casting of rounds with electromagnetic stirring, *ECOMAS* (2010).
[30] Bondeson, A., Rylander, T., and Ingelström, P. *Computational Electromagnetics*. Springer, (2010).
[31] Hon, Y. C., and Schaback, R. On unsymmetric collocation by radial basis functions, *Appl. Math. Comp.* (2001) **119**:177-186.